Inorganic Chemistry

Article

pubs.acs.org/IC

Structural, Spectroscopic, and Computational Studies on $Tl_4Si_5O_{12}$: A Microporous Thallium Silicate

Volker Kahlenberg,*[†] Lukas Perfler,[†] Jürgen Konzett,[†] and Peter Blaha[‡]

[†]Institute of Mineralogy and Petrography, University of Innsbruck, Innrain 52, A-6020 Innsbruck, Austria

[‡]Institute of Materials Chemistry, Vienna University of Technology, Getreidemarkt 9/165-TC, A-1060 Vienna, Austria

Supporting Information

ABSTRACT: Single crystals of the previously unknown thallium silicate $Tl_4Si_5O_{12}$ have been prepared from hydrothermal crystallization of a glassy starting material at 500 °C and 1kbar. Structure analysis resulted in the following basic crystallographic data: monoclinic symmetry, space group $C2/c$, a = 9.2059(5) Å, b = 11.5796(6) Å, c = 13.0963(7) Å, β = 94.534(5)°. From a structural point of view the compound can be classified as an interrupted framework silicate with Q^3- and Q^4-units in the ratio 2:1. Within the framework 4-, 6-, and 12-membered rings can be distinguished. The framework density of 14.4 T-atoms/1000 Å^3 is comparable with the values observed in zeolitic materials like Linde type A, for example. The thallium cations show a pronounced one-sided coordination each occupying the apex of a distorted trigonal TlO_3 pyramid. Obviously, this reflects the presence of a stereochemically active $6s^2$ lone pair electron. The porous structure contains channels running along [110] and [−1 1 0], respectively, where the Tl^+ cations are located for charge compensation. Structural investigations have been completed by Raman spectroscopy. The interpretation of the spectroscopic data and the allocation of the bands to certain vibrational species have been aided by DFT calculations, which were also employed to study the electronic structure of the compound.

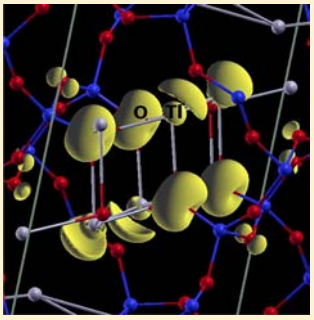

INTRODUCTION

Microporous thallium alumosilicates have been known for a long time. Among the group of zeolites, for example, several synthetic compounds have been reported which can incorporate large amounts of Tl^+. Examples include the following zeolite framework types: ABW,[1a,b] FAU,[2a−d] LTA,[3a−f] LTL,[4] MFI,[5] RHO,[6] SOD,[7] and ANA.[8] In most cases thallium containing *alumo*silicate zeolites were prepared from the Na analogues by ion exchange using aqueous solutions of a thallium salt such as $TlNO_3$ or Tl(OH) in the range between ambient temperature and 85 °C. ABW-type $TlAlSiO_4$ was obtained via hydrothermal reactions performed at 500 °C in sealed silver tubes using a high purity natural albite ($NaAlSi_3O_8$) and thallium nitrate solution as starting materials.[1b] Thallium-leucite ($TlAlSi_2O_6$) with ANA topology in turn has been synthesized from the transformation of dehydrated analcime ($NaAlSi_2O_6$) in the presence of a TlCl melt.[8]

Aluminum free thallium silicates with a three-dimensional tetrahedral framework structure have not been reported so far. Actually, the whole crystal chemistry of the phases belonging to the binary system Tl_2O-SiO_2 is rather uncharted territory. Until now, only $Tl_6Si_2O_7$ has been characterized in detail.[9a,b] This is even more surprising because a precise knowledge of the parameters that govern the stereochemical activity of the lone electron pairs in thallium(I) compounds is indispensable for the tailoring of their potential ferroelectric, pieozoelectric, and nonlinear optical properties or for the choice and design of complexing agents that can remove toxic thallium selectively from biological systems.[10] Thallium has been reported to be more poisonous to humans than mercury, cadmium, or lead due to its similarity to K^+ in cellular function. For example, in their 1996 report the World Health Organization recommends that the daily oral intake should be limited to approximately 10 μg of thallium. The average lethal oral dose for an adult has been estimated to be about as low as 10−15 mg/kg.[11a−c] However, thallium poisoning may also occur via inhalation or skin contact. The marked toxicity of thallium may be one of the reasons for the lack in structural information on thallium silicates.

Recently, we succeeded in the preparation of microporous alkali silicates such as γ-$Na_2Si_2O_5$ from low temperature devitrification of glassy precursors.[12] As a first result of a research project aimed at the synthesis of pure and mixed thallium-alkali silicates with this synthesis approach, a comprehensive characterization of the previously unknown framework compound $Tl_4Si_5O_{12}$ is reported in this contribution.

EXPERIMENTAL DETAILS

Synthesis. Starting material for the synthesis experiment was a stoichiometric mixture of dried Tl_2CO_3 (Merck, p.a.) and SiO_2 (AlfaAesar, 99.995%) in the molar ratio 1:2. A total of 300 mg was homogenized in an agate mortar under acetone, transferred to a platinum crucible, and subsequently covered with a lid. The crucible

Received: May 6, 2013
Published: July 8, 2013

   dx.doi.org/10.1021/ic401118s | *Inorg. Chem.* 2013, 52, 8941−8949

was fired from room temperature to 800 °C in a resistance heated furnace with a heating ramp of 5 °C/min. After a dwell time of 0.5 h the crucible was quenched in a water bath. The resulting pale yellow glass was mechanically removed from the container and crushed. Glass fragments with a weight of ∼30 mg were then loaded into a gold capsule (2.8/3.0 mm inner/outer diameter and 10 mm total length) and welded shut. Although no extra water was added to the glass, trace amounts of water adsorbed to the glass surface were present during the experiment. The high-P-T synthesis of the Tl silicate was performed using an externally heated Tuttle-type pressure vessel. At room temperature the sample was first taken to a pressure of 1 kbar and subsequently isobarically heated to 500 °C. After run duration of 18 days the sample was quenched to room conditions.

X-ray single crystal diffraction. A first inspection of the product using a polarized microscope indicated the presence of a glassy matrix in which (1) a larger number of idiomorphic quartz crystals (up to 200 μm in size) and (2) a small number of prismatic crystals having a considerably higher birefringence were embedded. A sample of this second phase showing sharp extinction when observed between crossed polarizers was selected for further structural investigation and mounted on the tip of a glass fiber using fingernail hardener. Single-crystal diffraction experiments were conducted on an Oxford Diffraction Gemini R Ultra diffractometer equipped with a Ruby CCD detector. A first determination of the lattice parameters resulted in a preliminary unit cell that was used for phase identification in the current Web-based version of the *Inorganic Crystal Structure Database* ICSD. Since search/match was unsuccessful, we decided to measure a full data set for structure determination. The parameters of this data collection are summarized in Table 1. Data reduction included Lorentz and polarization corrections. Furthermore, a multiscan absorption correction using spherical harmonics was applied. The reflections could be indexed with a monoclinic metric. Systematic absences indicated the diffraction symbol 2/*mC*−*c*−. Intensity statistics clearly pointed to the presence of a center of symmetry. Therefore, location of the heavy atoms was initiated in the centrosymmetric space group C2/*c* by Patterson methods (program SHELXS-86[13]). The structure was completed by difference Fourier calculations and consecutive least-squares refinement calculations using the program SHELXL-97[13] embedded in the WinGX program suite.[14] Structure determination revealed that the crystals correspond to a previously unknown thallium silicate phase with composition $Tl_4Si_5O_{12}$. Final full matrix least-squares refinement cycles including fractional coordinates as well as anisotropic displacement parameters for all atoms converged to a residual of R1 = 0.027 for 96 parameters and 1175 reflections with $I > 2\sigma(I)$ (see Table 1). An inspection of the structural model using the MISSYM subroutine of the program PLATON[15] revealed no indication for the choice of a space group of unnecessarily low symmetry. Refined atomic coordinates, anisotropic displacement parameters, and selected interatomic distances and angles are given in Tables 2−4, respectively. Figures showing structural details were prepared using the program ATOMS6.4.[16]

Table 1. Crystal Data and Structure Refinement for $Tl_4Si_5O_{12}$

empirical formula	$Tl_4Si_5O_{12}$
formula weight	1149.93
temperature	293(2) K
wavelength	0.71073 Å
crystal system	monoclinic
space group	C12/*c*1
unit cell dimensions	*a* = 9.2059(5) Å
	b = 11.5796(6) Å
	c = 13.0963(7) Å
	α = 90°
	β = 94.534(5)°
	γ = 90°
volume	1391.70(13) Å^3
Z	4
density (calcd)	5.488 Mg/m^3
abs coeff	46.659 mm^{-1}
F(000)	1960
crystal size	0.08 × 0.08 × 0.04 mm^3
theta range for data collection	2.83 to 26.35°.
index ranges	$-11 \le h \le 11$, $-14 \le k \le 14$, $-16 \le l \le 13$
reflns collected	4370
indep reflns	1407 [*R*(int) = 0.0418]
completeness to theta = 25.50°	99.6%
max and min transmission	0.2569 and 0.1180
refinement method	full-matrix least-squares on F^2
data/restraints/params	1407/0/96
goodness-of-fit on F^2	1.093
final *R* indices [$I > 2\text{sigma}(I)$]	R1 = 0.0287, wR2 = 0.0638
R indices (all data)	R1 = 0.0344, wR2 = 0.0657
largest diff peak and hole	1.368 and −1.901 e·Å^{-3}

Table 2. Atomic Coordinates (×10^4) and Equivalent Isotropic Displacement Parameters (Å^2 × 10^3) for $Tl_4Si_5O_{12}$[a]

	x	*y*	*z*	*U*(eq)
Tl(1)	3948(1)	4715(1)	6235(1)	18(1)
	3973	4790	6260	
Tl(2)	1679(1)	2026(1)	6331(1)	18(1)
	1671	1989	6334	
Si(1)	5577(2)	1954(2)	5822(2)	6(1)
	5505	1954	5795	
Si(2)	2258(2)	6072(2)	3981(2)	7(1)
	2229	6142	3944	
Si(3)	5000	104(3)	7500	6(1)
	5000	48	7500	
O(1)	5531(7)	874(6)	6585(5)	22(2)
	5376	808	6517	
O(2)	8659(6)	4307(5)	7084(4)	12(1)
	8583	4237	7183	
O(3)	4065(6)	2616(6)	5636(5)	16(1)
	4025	2703	5668	
O(4)	6070(7)	1452(6)	4751(5)	24(2)
	5905	1499	4659	
O(5)	6874(7)	2776(5)	6326(5)	17(1)
	6911	2664	6342	
O(6)	3330(7)	5088(6)	4410(5)	19(2)
	3318	5159	4408	

[a] *U*(eq) is defined as one-third of the trace of the orthogonalized U_{ij} tensor. The second line corresponds to the theoretical DFT calculations (*T* = 0 K).

Raman Spectroscopy. Confocal Raman spectra of the single crystal in the range of 50−4000 cm^{-1} were recorded with a Horiba Jobin Yvon Labram-HR 800 Raman microspectrometer. The complete spectrum in the range between 55 and 1500 cm^{-1} is given in Figure 1a. The samples were excited using the 532 nm emission line of a frequency-doubled 100 mW Nd:YAG laser under an Olympus 100× objective lens with a numerical aperture of 0.9. The size of the laser spot on the surface was approximately 1 μm. The scattered light was dispersed by an optical grating with 1800 lines mm^{-1} and collected by a 1024 × 256 open-electrode CCD detector. The spectral resolution, determined by measuring the Rayleigh line, was below 2 cm^{-1}. The spectra were recorded unpolarized at ambient conditions. The accuracy of the Raman line shifts, calibrated by regularly measuring the Rayleigh line, was on the order of 0.5 cm^{-1}. Background and Raman bands were fitted by the built-in spectrometer software LabSpec[1] to first- or second-order polynomial and convoluted

dx.doi.org/10.1021/ic401118s | *Inorg. Chem.* 2013, 52, 8941−8949

Table 3. Selected Bond Lengths [Å] (up to 3.2 Å) and Angles [deg] for $Tl_4Si_5O_{12}$[a]

Tl(1)−O(6)	2.451(7)	Si(1)−O(5)	1.625(6)
Tl(1)−O(3)	2.558(7)	Si(2)−O(6)	1.582(7)
Tl(1)−O(6)#1	2.716(7)	Si(2)−O(4)#6	1.607(6)
Tl(2)−O(3)	2.537(6)	Si(2)−O(5)#1	1.622(6)
Tl(2)−O(6)#4	2.633(7)	Si(2)−O(2)#1	1.631(6)
Tl(2)−O(3)#4	2.645(7)	Si(3)−O(1)	1.601(6)
Si(1)−O(3)	1.591(6)	Si(3)−O(1)#3	1.601(6)
Si(1)−O(1)	1.603(7)	Si(3)−O(2)#5	1.603(6)
Si(1)−O(4)	1.617(6)	Si(3)−O(2)#7	1.603(6)
O(6)−Tl(1)−O(3)	83.1(2)	O(6)−Si(2)−O(4)#6	114.3(4)
O(6)−Tl(1)−O(6)#1	80.2(2)	O(6)−Si(2)−O(5)#1	112.0(4)
O(3)−Tl(1)−O(6)#1	85.54(19)	O(4)#6−Si(2)−O(5)#1	107.7(4)
O(3)−Tl(2)−O(6)#4	95.5(2)	O(6)−Si(2)−O(2)#1	112.1(4)
O(3)−Tl(2)−O(3)#4	76.9(2)	O(4)#6−Si(2)−O(2)#1	106.2(3)
O(6)#4−Tl(2)−O(3)#4	78.1(2)	O(5)#1−Si(2)−O(2)#1	104.0(3)
O(3)−Si(1)−O(1)	113.9(3)	O(1)−Si(3)−O(1)#3	112.3(6)
O(3)−Si(1)−O(4)	110.0(4)	O(1)−Si(3)−O(2)#5	109.8(3)
O(1)−Si(1)−O(4)	106.5(4)	O(1)#3−Si(3)−O(2)#5	107.6(3)
O(3)−Si(1)−O(5)	112.7(4)	O(1)−Si(3)−O(2)#7	107.6(3)
O(1)−Si(1)−O(5)	105.0(4)	O(1)#3−Si(3)−O(2)#7	109.8(3)
O(4)−Si(1)−O(5)	108.4(3)	O(2)#5−Si(3)−O(2)#7	109.6(5)

[a]Symmetry transformations used to generate equivalent atoms: #1 $-x+1, -y+1, -z+1$; #2 $x+1/2, y+1/2, z$; #3 $-x+1, y, -z+3/2$; #4 $-x+1/2, -y+1/2, -z+1$; #5 $x-1/2, y-1/2, z$; #6 $x-1/2, y+1/2, z$; #7 $-x+3/2, y-1/2, -z+3/2$; #8 $x+1/2, y-1/2, z$.

Gaussian−Lorentzian functions, respectively (see also Figures 1b and 1c).

Theoretical Calculations. Density functional theory (DFT) based calculations using the generalized gradient corrected functional by Wu and Cohen[17] (WC-GGA) have been performed for $Tl_4Si_5O_{12}$ using the augmented plane wave plus local orbitals (APW+lo) method as incorporated in the WIEN2k code.[18] The atomic sphere radii (R_{MT}) for Tl, Si, and O were 2.3, 1.35, and 1.6 au, respectively. The wave functions in the atomic spheres were expanded as spherical harmonics up to angular momentum $l = 10$. Local orbitals were used for the semicore states (Tl-5d, Si-2p, and O-2s). In the interstitial region between the atomic spheres, a plane wave expansion was used, fixing the parameter $R_{MT}K_{max} = 6$, which is the product of the smallest atomic sphere radius and the largest plane wave K_{max}. The adequacy of the choice of the plane wave basis set size was checked by additional calculations using a larger $R_{MT}K_{max}$. A shifted k-mesh of $3 \times 5 \times 5$ points was used for the Brillouin zone summation. In the calculations the experimental lattice parameters were used, but the positions of the atoms were optimized simultaneously with the charge density during the self-consistency cycle[19] until the residual forces were smaller than 0.05 mRy/au. The Gamma-point phonons were calculated by a frozen phonon approach,[20] displacing the nonequivalent atomic positions by ±0.0567 au and calculating the corresponding forces. These forces are input to the PHONON program of Parlinski,[21] where the resulting force constants, the dynamical matrix, and the phonon frequencies were obtained.

RESULTS

Structural Aspects. In the crystal structure of $Tl_4Si_5O_{12}$ the [SiO_4] tetrahedra are linked into a three-dimensional so-called *interrupted* framework consisting of Q^3- and Q^4-groups in the ratio 2:1, i.e. the network simultaneously contains bridging and nonbridging oxygen atoms. The observed Si:O proportion of 5:12 (or 1:2.4) is very close to the originally intended 1:2.5 ratio of the synthesis. Whereas the latter value has been encountered in many single layer, double chain as well as a few double ring and framework silicates,[22] a silicate anion with a 5:12 ratio is rather exceptional and has been reported only once in the chain structure of the hydrous uranyl silicate mineral haiweeite.[23] The backbones of the framework structure of $Tl_4Si_5O_{12}$ are *dreier* double chains (see Figure 2) running parallel to [110] and [−1 1 0], respectively. Similar chains have been reported to exist as major building units in the crystal structures of synthetic $NaKSi_2O_5$ and the mineral okenite.[24a,b] The translation periods of about 7.397 Å along these chains correspond to the a_{RED} and b_{RED} lattice parameters of the corresponding triclinic primitive reduced cell. As can be seen from Figure 2 the double chains are characterized by a strictly alternating sequence of six- and four-membered rings. The sequence of directedness of up (U) and down (D) pointing tetrahedra within these two ring types is UUDD and UDUDUD, respectively. The double chains are located in layers parallel to (001) at $z = 0$ (for the chains parallel to [−1 1 0]) and $z = 1/2$ (for those parallel to [110]). Linkage between neighboring chains from different layers is provided by the four-connected tetrahedra around Si(3). The resulting three-dimensional network encloses central tunnels where the monovalent thallium cations are incorporated (see Figure 3).

The individual Si−O bond distances show a considerable scatter. Nevertheless, the observed values are in the normal range for silicate structures.[22] For the two three-connected (Q^3-type) tetrahedra around Si(1) and Si(2) the Si−O bond

Table 4. Anisotropic Displacement Parameters (Å² × 10³) for $Tl_4Si_5O_{12}$[a]

	U_{11}	U_{22}	U_{33}	U_{23}	U_{13}	U_{12}
Tl(1)	20(1)	21(1)	12(1)	−1(1)	1(1)	2(1)
Tl(2)	18(1)	21(1)	15(1)	−1(1)	1(1)	−1(1)
Si(1)	6(1)	9(1)	3(1)	2(1)	−1(1)	−1(1)
Si(2)	7(1)	11(1)	3(1)	0(1)	−3(1)	−2(1)
Si(3)	6(2)	6(2)	4(2)	0	−2(1)	0
O(1)	21(3)	20(4)	25(4)	17(3)	−1(3)	−3(3)
O(2)	10(3)	22(4)	3(3)	−2(3)	0(2)	−8(3)
O(3)	14(3)	17(3)	17(3)	−2(3)	−1(3)	2(3)
O(4)	27(4)	33(4)	11(3)	−11(3)	7(3)	−1(3)
O(5)	18(3)	11(3)	19(4)	2(3)	−7(3)	−10(3)
O(6)	20(3)	16(3)	20(4)	2(3)	−5(3)	0(3)

[a]The anisotropic displacement factor exponent takes the form $-2\pi^2[\, h^2a^{*2}U_{11} + \ldots + 2hka^*b^*\, U_{12}]$.

dx.doi.org/10.1021/ic401118s | Inorg. Chem. 2013, 52, 8941−8949

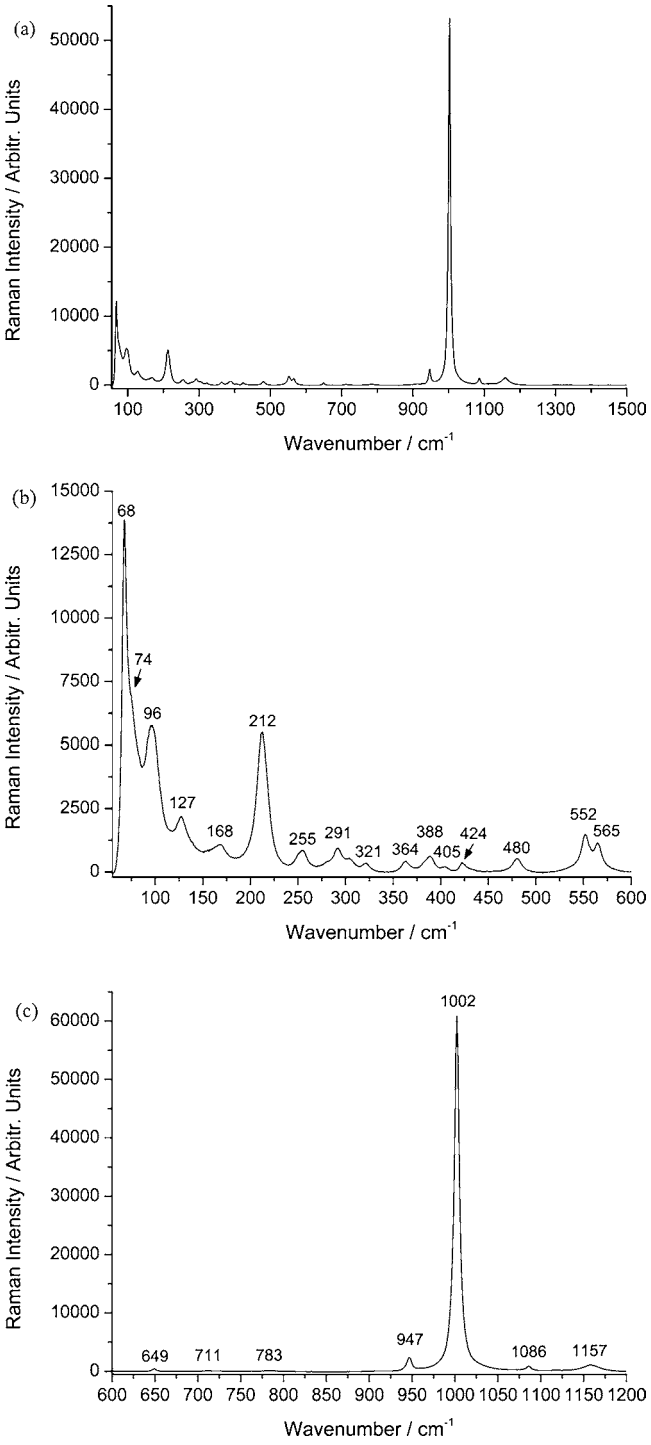

Figure 1. Unpolarized Raman spectrum of a $Tl_4Si_5O_{12}$ single crystal in the regions between (a) 55 and 1500 cm^{-1}, (b) 55 and 600 cm^{-1}, and (c) 600 and 1200 cm^{-1}.

distances to the nonbridging oxygen atoms O(3) and O(6) are significantly shorter than the bridging Si−O bonds, which average at about 1.615 Å and 1.620 Å, respectively. The shortening of the terminal bond lengths compared with the bridging bond lengths results from the stronger attraction between O and Si than between O and the nontetrahedral cations in the structure, and is a feature frequently observed for silicates. Contrary to Si(1) and Si(2), the Q^4-type Si(3)-tetrahedron residing on the special Wyckoff position 4*e* (site

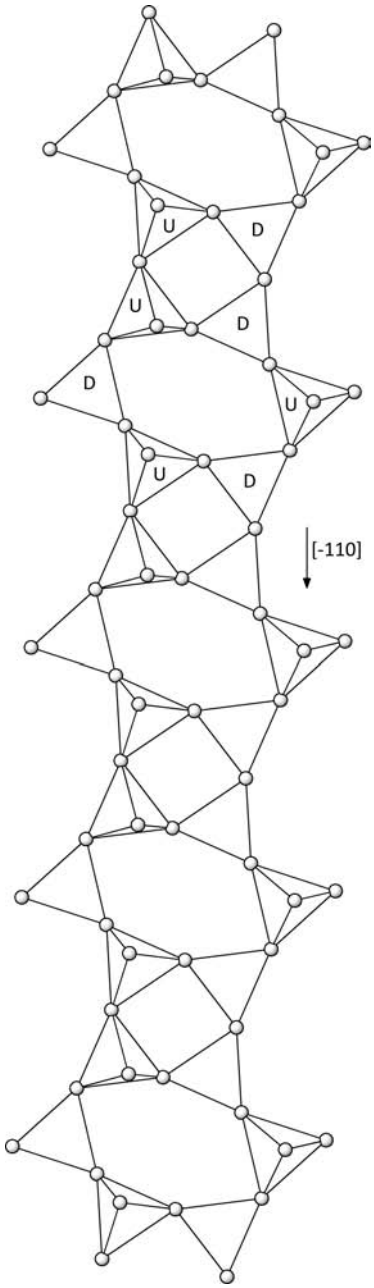

Figure 2. A single *dreier* double chain in the framework structure of $Tl_4Si_5O_{12}$ running parallel to [−1 1 0]. Small gray spheres represent oxygen atoms.

symmetry 2) has fairly uniform Si−O distances which average at about 1.602 Å . The O−Si−O bond angles range from 104° to 114°. These values are, again, rather typical of silicate structures.[22] The distortion of the tetrahedra can be expressed numerically by means of the quadratic elongation λ and the angle variance σ^2.[25] These parameters have the following values: 1.003 and 12.22 (for Si(1)), 1.004 and 16.15 (for Si(2)), and 1.001 and 3.02 (for Si(3)), i.e., the Q^4-tetrahedron about Si(3) shows the least degree of distortion.

The topology of the net (see also Figure 4) can be characterized by several indicators. The coordination sequences of the Si atoms, for example, have the following values: Si(1) and Si(2), 3−6−12−19−30−50−67−79−103−133; Si(3), 4−8−10−20−40−46−56−92−110−116. The resulting topological density calculated by adding the first 10 coordination

dx.doi.org/10.1021/ic401118s | Inorg. Chem. 2013, 52, 8941−8949

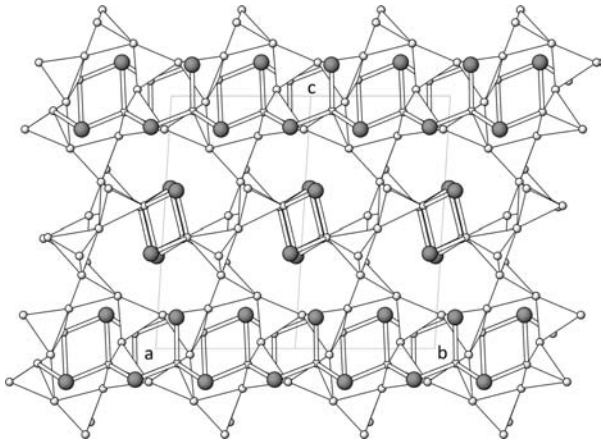

Figure 3. Projection of the whole framework structure parallel to [110]. Small (light) and large (dark) gray spheres represent oxygen and thallium atoms, respectively. Tl–O bonds are indicated.

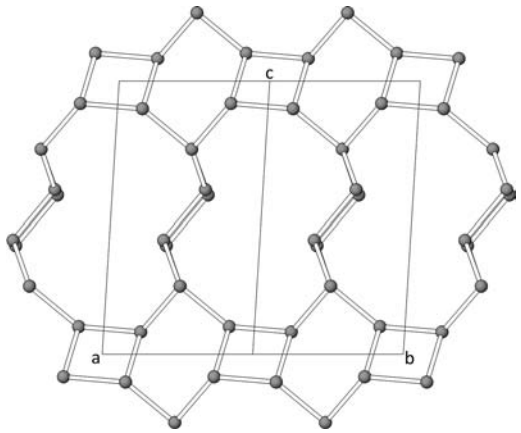

Figure 4. Topology of the net containing 4-, 6-, and 12-membered rings. Small gray spheres represent silicon atoms. Si–Si connections are indicated.

sequence numbers has a value of TD_{10} = 503. The vertex symbols[26] for the three tetrahedral centers are 4.8.6 (for Si(1) and Si(2)) and $12_5.6.12_5.12_5.6.12_5$ (for Si(3)). The framework density[27] of the porous crystal structure of $Tl_4Si_5O_{12}$ at room conditions is 14.4 T-atoms/1000 Å^3.

To fully describe the porous character of the network the structure has been analyzed using the web based program ZEOMICS.[28] The total volume of void (pore) space within the structure is 55% of the total volume or 0.346 cm^3/g. The derived pore size distribution indicates that the total pore volume has two types of contributions: channels with diameters <4 Å (15%) and cages with diameters <6 Å (85%). Of course, the *accessible* volume of a framework is a function of the molecule size. In the present case, for a minimum molecule diameter of 2 Å the total pore volume could be accessed. The *accessible* surface area for this diameter is about 255 m^2/g. Furthermore, two quantities are of particular interest for the characterization of the pores: the largest cavity diameter (LCD, the maximum of the pore size distribution) and the pore limiting diameter (PLD, the largest characteristic guest molecule size for which there is a nonzero accessible volume): The corresponding values are LCD = 5.0 Å and PLD = 3.0 Å, respectively. Concerning the values for the pore size distribution and the total pore volume, the present framework is comparable with the microporous zeolite framework type RWR.[28]

Charge balance in the structure is achieved by the two crystallographically independent thallium cations occupying general Wyckoff sites. Each of them is coordinated by three *primary* ligands belonging to the group of the nonbridging oxygen atoms O(3) and O(6). These Tl–O bond distances vary between 2.45 and 2.72 Å (average: 2.59 Å). In addition, between two (for Tl(1)) and three (for Tl(2)) much weaker *secondary* interactions exist with the bridging oxygens (Tl(1)–O_{brid}, 3.41–3.48 Å; Tl(2)–O_{brid}, 3.31–3.36 Å). Therefore, the thallium cations show a pronounced one-sided coordination each occupying the apex of a distorted trigonal TlO_3 pyramid. This reflects the presence of a stereochemically active $6s^2$ lone pair electron (LEP). In general, the stereochemical influence of the LEP on a $[LX_m]$ polyhedron (L: cation having one lone pair) can be approximately described using the so-called eccentricity parameter $\vec{\Phi}_i$, a vector which is defined as $\vec{\Phi}_i = -\sum_i \vec{\varphi}_{ij}$.[29a,b] Each $\vec{\varphi}_{ij}$ in turn is a vector directed from L_i to a specific ligand X_j. The length of $\vec{\varphi}_{ij}$ is defined as $|\vec{\varphi}_i| = \exp(-D_{ij}/g)$, where D_{ij} corresponds to the bond distance (in Å) between L_i and X_j and g represents an empirically determined constant having a value of 0.2 Å. The magnitude of the resulting vector $\vec{\Phi}_i$ is a measure for the deviation of the central cation from the geometrical point of gravity of the peripheral ions and its direction is given by the line from the nucleus of L_i to roughly the center of the deformation density of the LEP. The calculated $|\vec{\Phi}_i|$ values for Tl(1) and Tl(2) are 6.15×10^{-6} and 4.40×10^{-6}, respectively. Edge sharing $Tl(1)O_3$ and $Tl(2)O_3$ pyramids are linked in an alternating sequence into $^1_\infty[TlO]$ zigzag chains running parallel to the directions of the tetrahedral double chains (see Figure 5, which also indicates

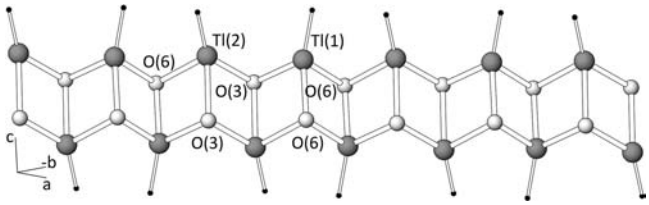

Figure 5. $^1_\infty[TlO]$ zigzag chains built up from the condensation of $Tl(1)O_3$ and $Tl(2)O_3$ pyramids. As a guide for the eye the approximate directions of the lone pair electrons are indicated by thin "bonds" linking the Tl cations with small black spheres.

the directions of the vectors $\vec{\Phi}_i$ for the two crystallographically independent Tl cations). In more detail, the pyramidal $^1_\infty[TlO]$ chains connect the tetrahedral double chains belonging the *same* layer at z = 0 or z = 1/2.

Bond valence calculations were performed with the bond distances of the first coordination sphere given in Table 3 using the parameters given by Brese and O'Keeffe[30] for the Si–O and the Tl–O pairs. The bond valence sums (BVS) for the cations are as follows: Si(1) 4.17 vu, Si(2) 4.15 vu, Si(3) 4.24 vu, Tl(1) 1.05 vu, and Tl(2) 0.93 vu. These values are close to the expected formal atomic valences of +4 and +1, respectively.

DFT Calculations. Starting from the experimental structural data, the atomic positions of all atoms were optimized in our DFT calculations. The theoretical positions (at T = 0 K) are also listed in Table 2. In general very good agreement between theory and experiment is found, in particular for the heavier atoms and when one considers that the experimental data refer

dx.doi.org/10.1021/ic401118s | Inorg. Chem. 2013, 52, 8941–8949

to room temperature. The corresponding bond lengths agree typically within 0.02−0.04 Å, where on average the Si−O bonds are 0.02 Å longer and the Tl(1)−O bonds are more isotropic in theory. From these distances BVS of 3.93, 3.89, and 4.04 follow for Si(1), Si(2), and Si(3); 0.78 and 0.74 for Tl(1) and Tl(2); and 2.04, 1.98, 1.72, 1.98, 1.95, and 1.65 for the six O-positions, respectively. The Si and O(1), O(2), O(4), and O(5) BVS are close to their formal valences, while Tl atoms have a smaller BVS, which is compensated by the smaller O(3) and O(6) BVS, i.e., those O-atoms which coordinate directly to Tl are less ionic.

For the analysis of the electronic structure and the bonding mechanism the partial density of states (DOS) is presented in Figure 6. Since the partial DOS of the two Tl and 3 Si positions

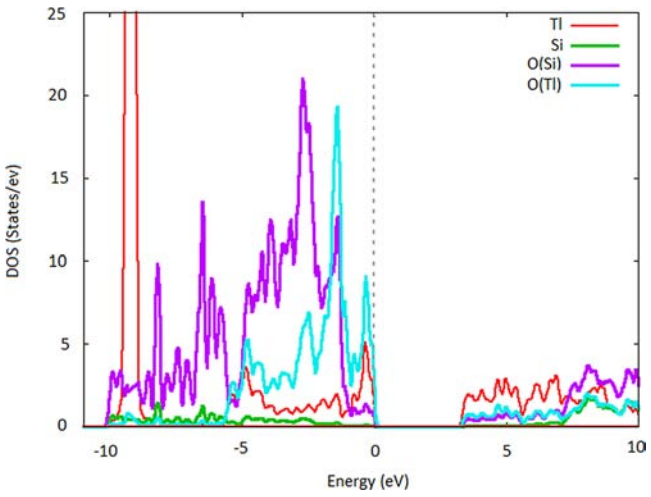

Figure 6. Partial DOS (according to their character within the corresponding atomic spheres).

are very similar, we have added them together. The partial DOS of the O atoms O(1), O(2), O(4), and O(5), which are connected only to Si (labeled O(Si)), is quite different from that of the O-atoms O(3) and O(6), which connect also to Tl (O(Tl)), and thus we show the partial DOS of these two distinct types of oxygen atoms. The Tl-5d states around −9.5 eV below the Fermi energy (E_F) form a narrow peak due to their spatial localization and weak hybridization, while the Tl-6s,6p valence state starts around −5.5 eV. The Si-3s,3p and O(Si)-2p orbitals form a 10 eV wide band, and the strong coincidence of their partial DOS visible in particular in the identical peak structure between −9 and −5 eV indicates strong covalent interactions between them (besides the obvious ionic bonding character). Between −5 eV and E_F the DOS of O(Si) and O(Tl) is very different, because O(Tl) hybridizes strongly with Tl states. The characteristic peaks around −5 eV and at the top of the valence band indicate bonding and antibonding character between O(Tl) and Tl states. In Figure 7 one can see that Tl-6s states dominate in the valence band and only near E_F some additional Tl-6p character is present, while in the conduction band Tl-6p states dominate.

In order to demonstrate the bonding and antibonding character of the O(Tl)−Tl interaction we show in Figure 8 the electron density of the states between −6 and −4 eV in a Si−O(Tl)−Tl plane. Obviously the O(Tl)-2p charge is strongly polarized toward Si, but there is also a positive electron density toward Tl indicating the overlap and bonding character between O(Tl)-2p and Tl-6s orbitals. On the other hand the

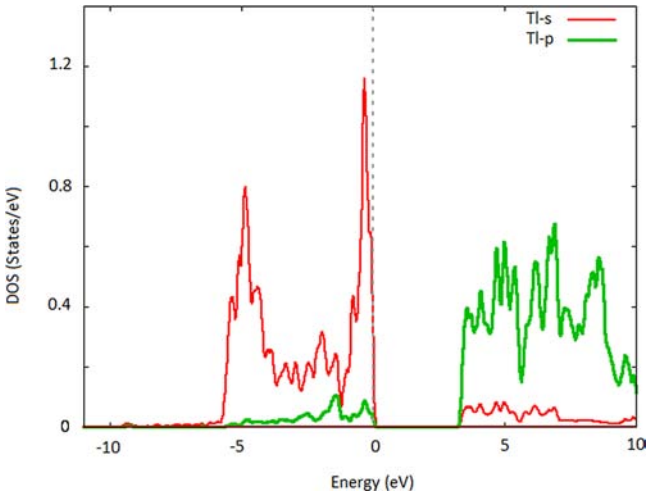

Figure 7. Partial DOS (Tl-s and p character).

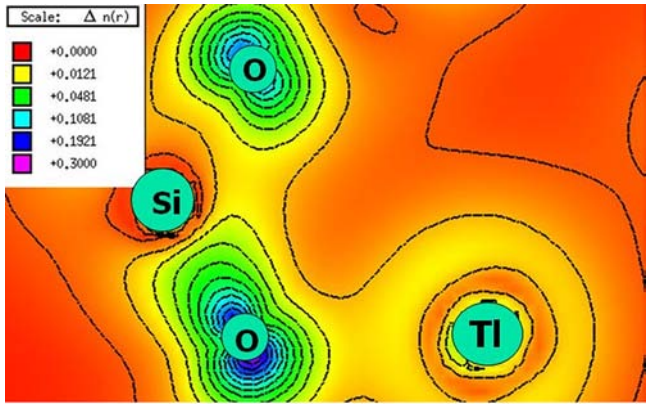

Figure 8. Electron density (in e^-/au^3) of the states between −6 and −4 eV (see partial DOS, Figures 6 and 7). It shows the bonding interaction between Tl and O.

states at the top of the valence bands (Figure 9) are antibonding between O(Tl) and Tl (zero density between these atoms) and the Tl density points into free space representing the expected lone pair of Tl. The lone pair of Tl can be seen even more clearly in the 3D isosurface plot in Figure 9.

Raman Spectroscopy. From the selection rules of factor group C_{2h} (space group $C2/c$) a total number of 126 vibrational modes are predicted for the monoclinic $Tl_4Si_5O_{12}$ with the irreducible representations $\Gamma = 31A_g + 31A_u + 32B_g + 32B_u$. These calculations on the monoclinic unit cell show that 63 modes ($31A_g + 32B_g$) are Raman-active while 63 modes ($31A_u + 32B_u$) are IR-active. As a result only nondegenerated modes are expected in the Raman spectrum of $Tl_4Si_5O_{12}$. Wavenumbers of the experimentally determined Raman bands and the calculated modes, their deviations, and the species of the vibration are listed in Table 5. Obviously it was experimentally not possible to find all Raman modes as required by the symmetry of this compound, because some Raman modes are so close together that they cannot be resolved. In addition, without polarized measurements on single crystals and theoretical intensity calculations the assignment of some of the experimental modes to the corresponding theoretical ones could be ambiguous. The average deviation of the calculated modes from the experimental values is 7 cm^{-1}, with a maximum

dx.doi.org/10.1021/ic401118s | Inorg. Chem. 2013, 52, 8941−8949

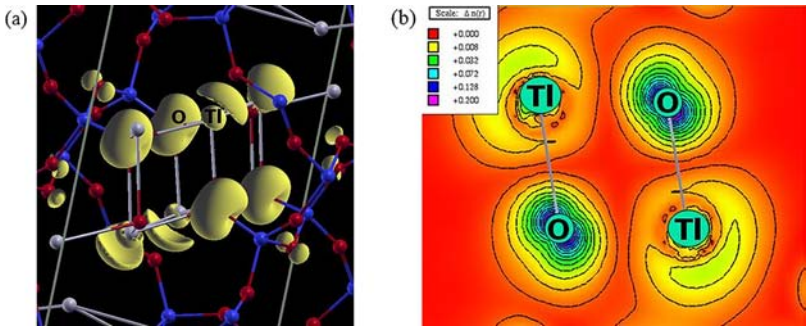

Figure 9. Electron density (in e^-/au^3) for states in an energy range between −1 eV and E_F (see partial DOS, Figures 6 and 7). The Tl lone pair is visible in both the 3D isosurface plot (a, left) and the contour plot in the Tl−O−Tl plane (b, right).

Table 5. Observed and Calculated Frequencies, Differences between Them, and Species of the Raman-Active Vibrational Modes in $Tl_4Si_5O_{12}$

$\tilde{\nu}_{exp}$ (cm^{-1})	$\tilde{\nu}_{calc}$ (cm^{-1})	$\tilde{\nu}_{exp-calc}$ (cm^{-1})	species	$\tilde{\nu}_{exp}$ (cm^{-1})	$\tilde{\nu}_{calc}$ (cm^{-1})	$\tilde{\nu}_{exp-calc}$ (cm^{-1})	species
68	67	1	B_g	388	382	6	B_g
	69		A_g	405	398	7	A_g
	71		A_g		412		A_g
74	72	2	B_g	424	415	9	B_g
83	81	2	B_g		435		B_g
	90		A_g		461		A_g
96	98	2	B_g	480	462	18	B_g
	103		A_g	552	539	13	A_g
114	115	1	B_g	565	556	9	B_g
127	130	3	A_g	649	629	20	A_g
	133		B_g		699		A_g
	140		A_g	711	711	0	B_g
168	171	3	B_g		752		B_g
	172		A_g		761		A_g
212	210	2	A_g	783	772	13	B_g
	217		B_g		936		A_g
	243		A_g	947	938	9	B_g
	245		B_g		978		A_g
255	264	9	B_g		981		B_g
281	277	4	A_g		985		B_g
291	293	2	A_g		993		A_g
306	309	3	B_g	1002	1005	3	A_g
321	346	25	A_g		1013		B_g
364	357	7	B_g		1068		B_g
	372		A_g	1086	1076	10	A_g
	380		B_g		1142		B_g
	381		A_g	1157	1143	14	A_g

deviation of 25 cm^{-1}. In Figure 10 the calculated partial phonon-DOS is given. As expected from the heavy mass, the Tl vibrations form a strong peak below 100 cm^{-1} and hardly contribute to vibrations above 170 cm^{-1}. Si vibrations dominate between 700 and 800 cm^{-1}, and a gap of about 100 cm^{-1} separates them from the O-stretching vibrations. Also in the phonons a strong difference between O(Tl) and O(Si) occurs and the O(Tl) contributions are at lower frequency, while the highest O(Si) vibrations reach up to 1150 cm^{-1}.

DISCUSSION

In his comprehensive monograph on the environmental impacts of thallium, Nriagu[31] lists more than 30 mineral species containing thallium. Most of them are sulfides (especially sulfosalts) as well as antimonides and selenides of

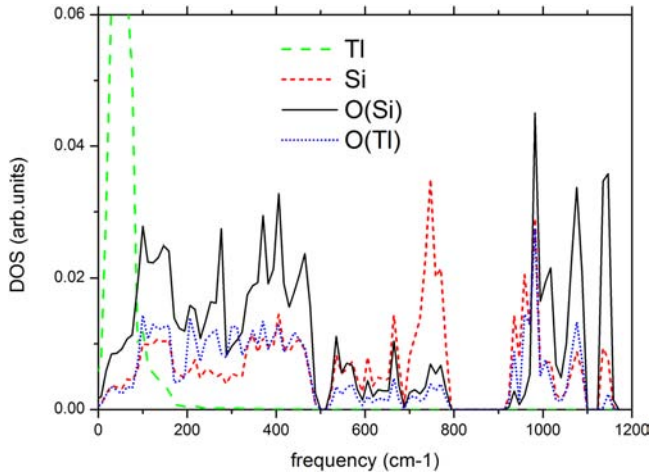

Figure 10. Partial phonon-DOS according to contributions of different atoms.

the thallous (Tl(I)) form. Examples of these minerals include lorandite ($TlAsS_2$), picotpaulite ($TlFe_2S_3$), or vrbaite ($Hg_3Tl_4As_8Sb_2S_{20}$). However, they are rather rare mineral species and not important rock forming minerals. Much more frequently thallium can be found as an impurity in sulfides such as galena (PbS) or sphalerite (ZnS) in concentrations of up to several thousand mg kg^{-1}.[32] Among the group of naturally occurring silicates Tl^+ is associated with minerals where it substitutes K^+. Examples include K-feldspar (up to 610 mg kg^{-1}) or layer silicates such as biotite or muscovite[33] (up to 350 mg kg^{-1}). So far no primary natural thallium silicate has been reported and, as already mentioned in the Introduction, among the synthetic anhydrous compounds also only one other representative is known: $Tl_6Si_2O_7$. At a first glance, it may appear that this sorosilicate and the interrupted framework silicate studied in our investigation do not have much in common. However, a more detailed look at the structural aspects reveals that distinct relationships can be found. The most pronounced is probably the existence of $^1_\infty[TlO]$ chains built up of $[TlO_3]$ pyramids in both structures. In $Tl_6Si_2O_7$ all the chains are parallel to each other—they are running along the hexagonal *c*-axis—whereas in $Tl_4Si_5O_{12}$ two differently oriented systems have to be distinguished. Actually, the $^1_\infty[TlO]$ chains are a structural building element that has been already observed in other oxothallate(I) compounds, for example in KTlO.[34]

Furthermore, we would like to emphasize that from a crystal chemical point of view the present compound is rather exotic. Actually, the number of corner sharing tetrahedral silicate

dx.doi.org/10.1021/ic401118s | Inorg. Chem. 2013, 52, 8941−8949

framework structures with quaternary (Q^4)- *and* tertiary (Q^3)-units is limited to a handful of phases including the title compound, $Na_2Si_3O_7$, $Na_2Si_3O_7{\cdot}H_2O$, $K_3NdSi_7O_{17}$, $Rb_6Si_{10}O_{23}$, and isotypic $Cs_6Si_{10}O_{23}$ as well as RUB-22 $(N(CH_3)_4)_4(Si_{32}O_{60}(OH)_{12})$.[35a−e] However, the proportion of the Q^4-sites in these phases differs significantly. In $K_3NdSi_7O_{17}$ only one in seven tetrahedra has four bridging oxygen ligands, whereas in $Na_2Si_3O_7$, $Na_2Si_3O_7{\cdot}H_2O$, and $Tl_4Si_5O_{12}$ one in three tetrahedra has four bridging oxygen ligands. Despite this principal similarity the sodium and thallium compounds represent different framework types. In RUB-22 half of the tetrahedra correspond to Q^4-sites, and in $Rb_6Si_{10}O_{23}$/$Cs_6Si_{10}O_{23}$ three out of five tetrahedra are four-connected. Extending this brief discussion to compounds with aluminum or beryllium on the T-sites, several zeolite-type materials as well as other natural framework phases also belong to this type of interrupted framework structures: wenkite $((Ba,K)_4(Ca,Na)_6(Al,Si)_{20}O_{41}(OH)_2(SO_4)_3{\cdot}H_2O)$, parthéite $(Ca_2Al_4Si_4O_{15}(OH)_2{\cdot}4H_2O)$, ussingite $(Na_2AlSi_3O_8(OH))$, maricopalite $(Pb_7Ca_2Al_{12}Si_{36}(O,OH)_{100}{\cdot}n(H_2O,OH))$, chiavennite $(CaMnBe_2Si_5O_{13}(OH)_2{\cdot}2H_2O)$, bavenite $(Ca_4Be_2Al_2Si_8O_{26}(OH)_2)$, leifite $(Na_7Be_2Al_3Si_{15}O_{39}F_2)$, telyushenkoite $(CsNa_6Be_2Al_3Si_{15}O_{39}F_2)$, and roggianite $(Ca_2BeAl_2Si_4O_{13}(OH)_2{\cdot}2.5H_2O)$.[36a−h] With regard to the extraframework cations, maricopalite is of special interest because it contains a large number of lone-pair cations (Pb^{2+}). Actually, the channels in the maricopalite structure host larger $Pb_4\phi_4$ clusters forming distorted cubes (ϕ: O, OH). Within a cluster every lead cation is connected to three next anion neighbors. These Pb−ϕ bond lengths are considerably shorter than the remaining Pb−O bond distances. Therefore, the principal bonding situation of a single Pb^{2+} cation is similar to the one of the Tl^+ ions in $Tl_4Si_5O_{12}$. However, in the present compound the $[TlO_3]$ groups are linked into chains and do not form clusters. Finally, we would like mention that the coordination environments of the thallium atoms in $Tl_4Si_5O_{12}$ are generally quite different from those observed in the Tl-exchanged sodium zeolites mentioned in the Introduction. After the ion exchange the Tl^+ ions occupy the positions where the sodium cations were located and, therefore, the Tl cations are usually significantly underbonded. The coordination sphere around the thallium atoms in $Tl_4Si_5O_{12}$ is much more appropriate to achieve a bond valence sum that is close to the valence of +1. The inert-pair effect of the Tl^+ cations can be sometimes detected (for example, in ABW-type $TlAlSiO_4$,)[1b] but it is significantly less pronounced than in $Tl_4Si_5O_{12}$.

Apart from being a crystal−chemical curiosity, the outcome of our study on $Tl_4Si_5O_{12}$ could be also of interest for the field of glass research. Nuclear magnetic resonance[37] as well as X-ray diffraction studies[38] revealed that thallium silicate glasses in the region of 15−35 mol % Tl_2O are characterized by the presence of thallium rich clusters (approximately 20 Å in diameter). Independent of the chemical composition of the glasses the analysis of the radial distribution functions[38] showed the presence of three Tl−Tl peaks at about 3.9, 7.0, and 10 Å. With this respect it is interesting to note that the Tl−Tl distances between next Tl neighbors in the pyramidal chains are in the range between 3.92 and 4.06 Å. This indicates that dimers of edge sharing TlO_3 pyramids could be the basic building units of these clusters.

■ ASSOCIATED CONTENT

Ⓢ Supporting Information

A CIF file with the relevant structural data. This material is available free of charge via the Internet at http://pubs.acs.org.

■ AUTHOR INFORMATION

Corresponding Author

*E-mail: volker.kahlenberg@uibk.ac.at.

Notes

The authors declare no competing financial interest.

■ ACKNOWLEDGMENTS

The authors are grateful to G. Diego Gatta and two other anonymous reviewers as well as the editor for their helpful comments and suggestions.

■ REFERENCES

(1) (a) Krogh, I. G.; Krogh, E.; Norby, P.; Colella, C.; De, M. *Zeolites* **1991**, *11*, 149−154. (b) Kyono, A.; Kimata, M.; Shimizu, M. *Am. Mineral.* **2000**, *85*, 1287−1293.

(2) (a) Kim, Y.; Han, Y. W.; Seff, K. *Zeolites* **1997**, *18*, 325−333. (b) Zhu, L.; Seff, K. *Micropor. Mesopor. Mat.* **2000**, *39*, 187−193. (c) Lim, W. T.; Seo, S. M.; Wang, L.; Lu, G. Q.; Heo, N. H.; Seff, K. *Micropor. Mesopor. Mat.* **2010**, *129*, 11−21. (d) Kim, J. J.; Kim, C. W.; Sen, D.; Heo, N. H.; Seff, K. *J. Phys. Chem. C* **2011**, *115*, 2750−2760.

(3) (a) Riley, P. E.; Seff, K.; Shoemaker, D. P. *J. Phys. Chem.* **1972**, *76*, 2593−2597. (b) Thöni, W. *Z. Kristallogr.* **1975**, *142*, 142−160. (c) Firor, R. L.; Seff, K. *J. Am. Chem. Soc.* **1977**, *99*, 4039−4044. (d) Subramanian, V.; Seff, K. *J. Phys. Chem.* **1979**, *83*, 2166−2169. (e) Cheetham, A. K.; Eddy, M. M.; Jefferson, D. A.; Thomas, J. M. *Nature* **1982**, *299*, 24−26. (f) Kim, D. S.; Song, S. H.; Kim, Y. *J. Korean Chem. Soc.* **1993**, *37*, 76−82.

(4) Artioli, G.; Kvick, A. *Eur. J. Mineral.* **1990**, *2*, 749−759.

(5) Huddersman, K. D.; Rees, L. V. C. *Zeolites* **1991**, *11*, 270−276.

(6) Parise, J. B.; Corbin, D. R.; Abrams, L.; Northrup, P.; Rakovan, J.; Nenoff, T. M.; Stucky, G. D. *Zeolites* **1994**, *14*, 25−34.

(7) Latturner, S. E.; Sachleben, J.; Iversen, B. B.; Hanson, J.; Stucky, G. D. *J. Phys. Chem. B* **1999**, *103*, 7135−7144.

(8) Kyono, A.; Kimata, M.; Shimizu, M.; Saito, S.; Nishida, N.; Hatta, T. *Mineral. Mag.* **1999**, *63*, 75−83.

(9) (a) Piffard, Y.; Marchand, R.; Tournoux, M. *Rev. Chim. Miner.* **1975**, *12*, 210−217. (b) Siidra, O. I.; Britvin, S. N.; Krivovichev, S. V.; Klimov, D. A.; Depmeier, W. *Glass Phys. Chem.* **2012**, *38*, 473−477.

(10) Mudring, A. Stereochemical activity of lone pairs in heavier main-group element compounds. In *Inorganic Chemistry in Focus III*; Meyer, G., Naumann, D., Wesemann, I., Eds.; Wiley-VCH: New York, 2006; pp 15−28.

(11) (a) http://www.inchem.org/documents/hsg/hsg/hsg102.htm#PartNumber:3. (b) Peter, A. L. J.; Viraraghavan, T. *Environ. Int.* **2005**, *31*, 493−501. (c) Schoer, J. Thallium. In *The handbook of environmental chemistry. Vol. 3. Anthropogenic compounds. Part C*; Hutzinger, O., Ed.; Springer-Verlag: Berlin; pp 143−214, 1984.

(12) Kahlenberg, V.; Rakić, S.; Weidenthaler, C. *Z. Kristallogr.* **2003**, *218*, 421−431.

(13) Sheldrick, G. M. *Acta Crystallogr., Sect. A* **2008**, *64*, 112−122.

(14) Farrugia, L. J. *J. Appl. Crystallogr.* **1999**, *32*, 837−838.

(15) Spek, A. L. *PLATON, A Multipurpose Crystallographic Tool*; Utrecht University: Utrecht, The Netherlands, 1998.

(16) Dowty, E. *ATOMS, Version 6.4*; Shape Software: Kingsport, TN, 2011.

(17) Wu, Z.; Cohen, R. *Phys. Rev. B* **2006**, *73*, 235116.

(18) Blaha, P.; Schwarz, K.; Madsen, G.; Kvasnicka, D.; Luitz, J. *WIEN2k: An Augmented Plane Wave + LO Program for Calculating Crystal Properties*, TU Wien: Vienna, 2001.

(19) Marks, L. D. *Phys. Rev. B* **2013**, in press.

(20) Parlinski, K.; Li, Z. Q.; Kawazoe, Y. *Phys. Rev. Lett.* **1997**, *78*, 4063.

(21) Parlinski, K. *Software PHONON*; Cracow, 2013.
(22) Liebau, F. *Structural Chemistry of Silicates; Structure, Bonding and Classification*; Springer-Verlag: Berlin, 1985.
(23) Burns, P. C. *Can. Mineral.* **2001**, *39*, 1153−1160.
(24) (a) Rakić, S.; Kahlenberg, V. *Solid State Sci.* **2001**, *3*, 659−667. (b) Merlino, S. *Am. Mineral.* **1983**, *68*, 614−622.
(25) Robinson, K.; Gibbs, G. V.; Ribbe, P. H. *Science* **1971**, *172*, 567−570.
(26) O'Keefe, M.; Hyde, S. T. *Zeolites* **1997**, *19*, 370−374.
(27) Brunner, G. O.; Meier, W. M. *Nature* **1989**, *337*, 146−147.
(28) First, E. L.; Goumaris, C. E.; Wei, J.; Floudas, C. A. *Phys. Chem. Chem. Phys.* **2011**, *13*, 17339−17358.
(29) (a) Wang, X.; Liebau, F. *Z. Kristallogr.* **1996**, *211*, 437−439. (b) Wang, X.; Liebau, F. *Acta Crystallogr., Sect. B* **2007**, *63*, 216−228.
(30) Brese, N. E.; O'Keeffe, M. *Acta Crystallor., Sect. B* **1991**, *47*, 192−197.
(31) Nriagu, J. O. *Thallium in the Environment*; John Wiley: New York, 1998.
(32) Wedepohl, K. H., Ed. *Handbook of Geochemistry*; Springer-Verlag: Berlin-Heidelberg-New York, 1974; Vol. *2*, Part 4.
(33) Jović, V. Thallium. In *Encyclopedia of Geochemistry*; Marshall, C. P., Fairbridge, R. W., Eds. Kluwer Academic Press Publishers: Dordrecht, 1999; pp 622−623.
(34) Sabrowsky, H. *Z. Anorg. Allg. Chem.* **1978**, *438*, 213−221.
(35) (a) Kahlenberg, V.; Marler, B.; Munoz Acevedo, J. C.; Patarin, J. *Solid State Sci.* **2002**, *4*, 1285−1292. (b) Matijasic, A.; Marler, B.; Patarin, J. *Int. J. Inorg. Chem.* **2000**, *2*, 209−216. (c) Haile, S. M.; Wuensch, B. J. *Acta Crystallogr., Sect. B* **2000**, *56*, 773−779. (d) Schichl, H.; Völlenkle, H.; Wittmann, A. *Monatsh. Chem.* **1973**, *104*, 854−863. (e) Latzel, S.; Marler, B.; Oberhagemann, U.; Osterhoff, C.; Gies, H. *Stud. Surf. Sci. Catal.* **2007**, *170A*, 199−205.
(36) (a) Merlino, S. *Acta Crystallogr., Sect. B* **1974**, *30*, 1262−1266. (b) Engel, N.; Yvon, K. *Z. Kristallogr.* **1984**, *169*, 165−174. (c) Rossi, G.; Tazzoli, V.; Ungaretti, L. *Am. Mineral.* **1974**, *59*, 335−340. (d) Rouse, R. C.; Peacor, D. R. *Am. Mineral.* **1994**, *79*, 175−184. (e) Tazzoli, V.; Domeneghetti, M. C.; Mazzi, F.; Cannillo, E. *Eur. J. Mineral.* **1995**, *7*, 1339−1344. (f) Cannillo, E.; Coda, A.; Fagnani, G. *Acta Crystallogr.* **1966**, *20*, 301−309. (g) Sokolova, E.; Huminicki, D. M. C.; Hawthorne, F. C.; Agakhanov, A. A.; Pautov, L. A.; Grew, E. S. *Can. Mineral.* **2002**, *40*, 183−192. (h) Giuseppetti, G.; Mazzi, F.; Tadini, C.; Galli, E. *N. Jb. Mineral. Mh.* **1991**, *1991*, 307−314.
(37) Panek, L. W.; Bray, P. J. *J. Chem. Phys.* **1977**, *66*, 3822−3831.
(38) Milberg, M. E.; Peters, C. R. *Phys. Chem. Glasses* **1969**, *10*, 46.